

## ORIGINAL ARTICLE



# Utilization of GelMA with phosphate glass fibers for glial cell alignment

Zalike Keskin-Erdogan<sup>1</sup> | Kapil D. Patel<sup>2,3,4</sup> | David Y.S. Chau<sup>1,2,3</sup> |  
Richard M. Day<sup>5</sup> | Hae-Won Kim<sup>2,3,4,6</sup> | Jonathan C. Knowles<sup>1,2,3</sup>

<sup>1</sup>Division of Biomaterials and Tissue Engineering, Eastman Dental Institute, University College London, Royal Free Hospital, London, UK

<sup>2</sup>UCL Eastman-Korea Dental Medicine Innovation Centre, Dankook University, Cheonan, Republic of Korea

<sup>3</sup>Department of Nanobiomedical Science & BK21 PLUS NBM Global Research Center for Regenerative Medicine Research Center, Dankook University, Cheonan, Republic of Korea

<sup>4</sup>Institute of Tissue Regeneration Engineering (ITREN), Dankook University, Cheonan, Republic of Korea

<sup>5</sup>Centre for Precision Healthcare, UCL Division of Medicine, University College London, London, UK

<sup>6</sup>Department of Biomaterials Science, College of Dentistry, Dankook University, Cheonan, Republic of Korea

## Correspondence

Jonathan C. Knowles, Division of Biomaterials and Tissue Engineering, Eastman Dental Institute, University College London, Royal Free Hospital, Rowland Hill Street, NW3 2PF London, UK  
Email: j.knowles@ucl.ac.uk

## Funding information

Republic of Turkey Ministry of National Education, Grant/Award Number: YLSY-2016; National Research Foundation of Korea, Grant/Award Numbers: 2018K1A4A3A0106425, 2018R1D1A1B07048020

## Abstract

Glial cell alignment in tissue engineered constructs is essential for achieving functional outcomes in neural recovery. While gelatin methacrylate (GelMA) hydrogel offers superior biocompatibility along with permissive structure and tailorable mechanical properties, phosphate glass fibers (PGFs) can provide physical cues for directionality of neural growth. Aligned PGFs were fabricated by a melt quenching and fiber drawing method and utilized with synthesized GelMA hydrogel. The mechanical properties of GelMA and biocompatibility of the GelMA-PGFs composite were investigated *in vitro* using rat glial cells. GelMA with 86% methacrylation degree were photo-crosslinked using 0.1%wt photo-initiator (PI). Photocrosslinking under UV exposure for 60 s was used to produce hydrogels (GelMA-60). PGFs were introduced into the GelMA before crosslinking. Storage modulus and loss modulus of GelMA-60 was  $24.73 \pm 2.52$  and  $1.08 \pm 0.23$  kN/m<sup>2</sup>, respectively. Increased cell alignment was observed in GelMA-PGFs compared with GelMA hydrogel alone. These findings suggest GelMA-PGFs can provide glial cells with physical cues necessary to achieve cell alignment. This approach could further be used to achieve glial cell alignment in bioengineered constructs designed to bridge damaged nerve tissue.

## KEYWORDS

aligned growth, glass fibers, hydrogel, photo-crosslinking

## 1 | INTRODUCTION

Severe trauma in the central nervous system (CNS) can cause significant nerve injury with loss of tissue integrity and function at the injury

site. Moreover, neuronal and glial cells can die at the site of injury due to shearing, failure of ionic homeostasis, and loss of membrane integrity.<sup>1</sup> However, several supportive cells such as astrocytes, microglia, and oligodendrocytes near the injury site survive and collective

This is an open access article under the terms of the Creative Commons Attribution License, which permits use, distribution and reproduction in any medium, provided the original work is properly cited.

© 2021 The Authors. *Journal of Biomedical Materials Research Part A* published by Wiley Periodicals LLC.

interactions of these surviving cells can start the CNS repair and regeneration process. Due to the various challenges in neural regeneration processes such as slow axonal regeneration and inhibitory effects of the injured environment, the nerve recovery rate is very slow and can take a significant period of time in this complex biological environment.<sup>2-4</sup> Particularly, after major spinal cord injuries (SCI) substantial tissue loss may occur and result in a fluid-filled cavity, astrocyte reactivity, and glial scar formation at the injured site which may even propagate over time and lead to further secondary tissue damage.<sup>5</sup>

Over the past few decades, various types of biomaterial scaffolds, processed by methods such as electrospun nanofibers,<sup>6</sup> freeze dried/solvent cast,<sup>7</sup> self-assembly, gas foaming and hydrogels<sup>8-11</sup> have been investigated for neural tissue regeneration. These studies suggest that polymer-based biomaterial scaffolds can be used to repair CNS injury, alter the microenvironment of lesions, and promote the recovery of neural function.<sup>12</sup> Recently, hydrogel-based biomaterials have gained significant attention in CNS as well as peripheral nerve system (PNS) regeneration applications due to low cost, easy processing, controlled mechanical properties, permeability, and by serving as carriers for bioactive molecules and cell delivery to provide a permissive environment for regeneration. Moreover, hydrogels can mimic the extracellular matrix (ECM) to provide a niche for cells, support the surrounding neural tissue and also act as a substrate for cell growth, neurite formation, and axon regeneration.<sup>10</sup> The high-water content and porous inner structure help long-term nutrient supply for cells and thus can aid in axon survival.<sup>13</sup> Numerous studies have indicated that hydrogels can promote cell adhesion, axon regeneration, and myelination in neural damage both *in vitro* and *in vivo*.<sup>14-16</sup> Although hydrogel-based biomaterials possess superior biological properties, there are some drawbacks to natural hydrogels (such as collagen, fibrin, hyaluronic acid, and gelatin) as their mechanical properties are mostly dependent on polymerisation and the crosslinking mechanism and it can be difficult to control the microstructure and reproducibility between experiments. Compared to natural hydrogels, synthetic hydrogels offer more flexibility for closely defining the chemical composition and mechanical properties. Combining natural and synthetic hydrogels as hybrid materials or using naturally derived semi synthetic hydrogels such as Gelatin-methacry(ate)/(loyl) (GelMA) hold great potential in tissue engineering applications. GelMA is a semi-synthetic hydrogel, which consists of gelatin coupled with methacrylamide (MA) and the methacrylate groups enables the exploitation of the biological signals inherent in the gelatin molecule, while allowing control of mechanical properties.<sup>17,18</sup> Moreover, GelMA has shown important features such as enzymatic degradation in response to matrix metalloproteinases (MMPs), biocompatibility, cell adhesion due to presence of arginine-glycine-aspartic acid sequence (RGD) and controllable biophysical properties.<sup>19</sup> GelMA-based hydrogels have been investigated vastly for potential use in tissue engineering, drug delivery, and 3D bioprinting applications.<sup>20-22</sup>

Phosphate-based glasses are mainly composed of  $P_2O_5$  as glass network former,  $Na_2O$  and  $CaO$ .<sup>23</sup> Modifying oxides such as  $SrO$ ,  $TiO_2$ ,<sup>24,25</sup>  $Ag_2O$ ,<sup>26</sup>  $Fe_3O_4$ ,<sup>27</sup>  $ZnO$ ,  $CeO_2$ ,<sup>28</sup> and  $CuO$ <sup>29</sup> have been

included to induce the specific properties such as antibacterial, antioxidant, and anti-inflammatory properties, and other biological responses. Phosphate-based glasses have been studied to examine their potential for biomaterial applications mainly in bone tissue engineering, and drug and therapeutic ions such as copper, and silver delivery.<sup>25</sup> Phosphate glass fibers (PGFs) are biocompatible and biodegradable, and their tuneable degradation rate can be easily achieved by altering the compositions of phosphorus pentoxide, sodium oxide and calcium oxide within the glass network. Moreover, PGFs have shown excellent properties as guidance systems especially for the regeneration of outgrowing axons.<sup>27</sup> PGFs can promote highly directional growth of neurites *in vitro* and three-dimensional (3D) scaffolds with fibers facilitated the rate of directional axonal outgrowth in the *in vivo* sciatic nerve transection model.<sup>30</sup>

Up to date nerve guidance systems have been evaluated on mostly peripheral nerves and also with spinal cord. In more detail, both for peripheral nerves and SCI the outer structure of an implantable scaffold is usually tubular in order to bridge up disconnected tissue, while its inner structures should be designed such that injured axons can migrate into it from both proximal and distal stumps following transection. From the perspective of axonal regeneration, providing physical cues for alignment to the fibrous scaffolds are ideal for surrounding cells' and ultimately axonal guidance.<sup>30</sup> Particularly for CNS glial cells are aroused interest for their crucial roles as supportive cells for neural tissue by providing optimal environment and function for neurons,<sup>31</sup> thus glial cells are subjected into this work as potential treatment elements.

This study aimed to evaluate the combination of PGFs and GelMA and to design an effective 3D scaffold as a potential cell carrier for spinal tissue engineering that potentially can provide directionality and a permissive environment for growth of glial cells.

## 2 | MATERIALS AND METHODS

### 2.1 | Production and characterization of PGFs

The quaternary glass compositions of  $(50P_2O_5-40CaO-5Na_2O, 5Fe_2O_3, \text{ mol.}\%)$  were produced using precursors chemicals of  $NaH_2PO_4$ ,  $P_2O_5$ ,  $CaCO_3$ ,  $Fe_2O_3$  (Sigma-Aldrich, UK). The chemicals were mixed and then placed in a 200 mL platinum/ 5% rhodium (Pt/5% Rh) crucible (Type 71040, Johnson Matthey, UK) and heated in a furnace (Carbolite, model RHF 1500, UK) in air at  $700^\circ\text{C}$  for 30 min and then melted at  $1100^\circ\text{C}$  for 1 h. After that, the melted glass was poured onto a steel plate and left to cool to room temperature. Using this glass, the fibers were produced using a continuous, fiber drawing method as previously reported.<sup>27</sup> For glass compositions, the drum (collector) pulling speed was at 800 m/min. To measure the fiber diameter, a small bundle of parallel-aligned fibers was placed into a polytetrafluoroethylene (PTFE) mould and covered with resin (SpeciFix-20 kit Resin, Struers). The resin was ground and polished to examine under a microscope that attached to a CoolSnap Digital Image Analysis. Image Pro Plus software was used to measure the

diameter of the fibers in microns. The mean values and errors were calculated from measurements on 55 fibers. This value was also confirmed via scanning electron microscopy (SEM; Philips XL30 field emission SEM, Netherlands) of the fibers. As an inorganic material, PGFs did not require sample coating.

## 2.2 | Degradation of PGFs and ion release test

Degradation experiments were conducted on the glass fibers. From the same bundle of glass fibers, 1 cm long samples were cut and immersed in 3 mL of ultra-pure water (UPW) (10 mg/mL). All samples were incubated in an incubator at 37°C for 1, 3, 5, 7, 14, 21, 28 days and supernatants of samples were collected to conduct inductively coupled plasma-optical emission spectroscopy (ICP-OES) (Agilent Technologies-Varian 720-ES, Santa Clara, CA 95051, US) to detect released ion concentrations and the remains of the fibers were collected and dried at 37°C for 12 h to determine the change at corresponding time points. For all time points, three replicates were measured (Ohaus PA224 Pioneer Analytical Balance, UK), and the average mass change was calculated by the formula of

$$\% \text{weight change} = \frac{\text{final dry weight of PGFs} - \text{initial dry weight of PGFs}}{\text{initial dry weight of PGFs}} * 100$$

## 2.3 | Cytotoxicity and biocompatibility of PGF

Cytotoxicity of the PGFs was assessed using an elution-extraction method based on a protocol adapted from ISO10993-5 standard test method<sup>32</sup> with L929 mouse fibroblasts cells and rat C6 glioma cell line. L929 cells were cultured in Dulbecco's modified eagle medium (DMEM; Gibco™, Thermo-Fischer Scientific, UK) and C6 cells were cultured in F-12 K (ATCC® 30-2004™, USA) supplemented with 10% fetal bovine serum (FBS) (for DMEM) or 10% horse serum (HS) plus 5% FBS (for C6), 2 mM L-glutamine, 100 U/mL penicillin, and 100 µg/mL streptomycin (PS)- hereafter referred to as "complete medium"- in a humidified incubator at 37°C in 5% CO<sub>2</sub>. The PGFs were incubated in the culture medium (0.2 g sample/ml) without FBS supplement (extraction medium) for 24 h at 37°C in 5% CO<sub>2</sub>.

Both types of cell were cultured in 96 well tissue culture plates (1 × 10<sup>4</sup> cells/well) in complete medium until cells attained >90% confluency. The medium was replenished with the extraction medium (undiluted, with the ratio of 1:2 and 1:4 diluted in fresh medium). The control group consisted of cells supplemented with medium without addition of serum. The cells were incubated for a further 24 h at 37°C in 5% CO<sub>2</sub>. The metabolic activity of the cells was determined using an alamarBlue assay (DAL1025, Thermo Fisher Scientific, UK). The assay dye was added at 10% v/v to each well and incubated for 4 h at 37°C in the dark. The fluorescence intensity of each well was measured using a fluorescence plate reader (Labsystems, Helsinki, Finland; ex 530 nm / em 590 nm). The ratio of fluorescence intensity of the

reduced alamarBlue compared with the control (Thermanox plastic coverslips, Thermo Fisher Scientific, UK) allowed calculation of relative cell metabolic activity.

The biocompatibility of PGF was further assessed using C6 (ATCC® CCL-107™) rat glial cells seeded on glass fiber surfaces. Bundles of PGFs (0.1 g, 1 cm length) were sterilized in an oven at 110°C for 1 h then placed in low attachment cell culture plates. Cells (total of 1 × 10<sup>4</sup> cells) was added to the PGF bundles and incubated at 37°C in 5% CO<sub>2</sub> for 1 h to allow cell attachment then complete F-12 K culture media added. Cell viability was analyzed by Live/Dead® cell imaging kit (Thermo Scientific, UK) at day 7. Imaging was performed on confocal laser scanning microscopy (BioRad Radiance2100, Zeiss, UK). The images were reconstructed using ImageJ® (NIH, USA) software. Ultra-structural analysis of the interaction of C6 cells with PGF surface was conducted using scanning electron microscopy (SEM). Samples were fixed in 2.5% glutaraldehyde solution in 0.1 M sodium cacodylate (CAC) buffer, dehydrated in ethanol serial diluted solutions (20–100% v/v) for 10 min consecutively. Before critical point drying, samples were immersed in hexamethyldisilazane (Sigma Aldrich, UK) for 2 min and sputter-coated with gold (Polaron E5000) for imaging.

## 2.4 | GelMA production and characterization

The GelMA synthesis method has been modified from Zhu et al.<sup>20</sup> Briefly, to obtain GelMA, 10% wt/v of gelatin (Sigma-Porcine skin 300 bloom, Type A, UK) was dissolved in 0.1 M carbonate bicarbonate (CB) buffer pH 9.4 at 55°C under magnetic stirring at 300–400 rpm. Methacrylic anhydride (MA) (MAA, 94% Sigma-Aldrich, UK) was added into the gelatin solution at concentration of 0.1 mL MAA/g gelatin at a rate of 0.5 mL/min while stirring at 55°C. After 2 h reaction in the dark, the synthesis was stopped by neutralising the pH to 7.4 using drops of 6 M of HCl acid. Finally, the product was dialyzed against deionized water for five days with several water replacements at 40°C using a cellulose tubing dialysis membrane (12.4 kDa Molecular Weight Cut-off, Sigma-Aldrich, UK) to remove salts and unreacted excess free methacrylic acids. The obtained solution of GelMA was freeze-dried and collected in foam form and stored at 4°C for future experiments. To prepare GelMA hydrogel, the concentration was kept at 10% w/v by dissolving the stored GelMA foam form in PBS at 37°C. Crosslinking of the hydrogel solution was performed using 0.1% w/v PI of lithium phenyl-2,4,6-trimethylbenzoylphosphinate (LAP; >95%, Sigma-Aldrich, UK) and GelMA was solution cast while warm into the desired well plate then allowed to rest at 4–10°C for 10 min to form a gel prior to final crosslinking with ultraviolet light (UV; XYZPrinting UV chamber, Model 3UD10, Taiwan, UV LED λ 375–405 nm, 16 W) for 60 s throughout the study unless otherwise stated.

## 2.5 | Degree of substitution (DS) – <sup>1</sup>H-NMR

To measure degree of substitution of MA modified gelatin, <sup>1</sup>H nuclear magnetic resonance (Bruker Avance Neo 700, USA) was performed.

10–20 mg of gelatin, synthesized GelMA and commercial GelMA (Sigma, 900496-1G, UK) were dissolved in 1 mL of deuterated dimethyl sulfoxide (DMSO; Sigma, D2650, UK) at room temperature. The degree of methacrylation (DM) of GelMA samples which is the percentage of  $\epsilon$ -amino groups of gelatin modified with MA, was calculated by using Equation (1) and evaluated by calculating the peak area ratio of modified amino groups to primary amino groups.<sup>33</sup> For interpretation of <sup>1</sup>H-NMR results the TopSpin™ software of Bruker were used. Before the interpretation, phase corrections were applied to all spectra to obtain purely absorptive peaks, and baselines were corrected.

$$DM(\%) = 1 - \left( \frac{\text{GelMA Lysine methylene area}}{\text{Gelatin Lysine methylene area}} \right) * 100$$

## 2.6 | ATR-FTIR characterization

Chemical structures of gelatin, GelMA, PGFs and GelMA-PGFs were assessed by attenuated total reflectance Fourier transform infrared spectroscopy (ATR-FTIR, System 2000, PerkinElmer, Seer Green, UK) over a range of 4000–400  $\text{cm}^{-1}$  with a resolution of 4  $\text{cm}^{-1}$  and presented in spectra with the area of interest of 2000–600  $\text{cm}^{-1}$ . The absorption peaks and frequencies of specific chemical groups and the methacrylation of gelatin were detected by FTIR.

## 2.7 | Mechanical characterization

GelMA was cast into 96 well plates as described in 2.4., specifically for mechanical characterization. Meniscus formation on the top surface was avoided while casting GelMA by careful pipetting and when it occurred gels were gently cut to provide flat upper surface prior to testing. The mechanical properties of GelMA and GelMA-PGFs hydrogels with a diameter of  $\sim 6.5$  mm and a thickness of  $\sim 4.0$  mm with flat surfaces were characterized using dynamic mechanical analyser (DMA; Discovery DMA 850, TA Instruments, New Castle, USA) at room temperature. For GelMA-PGFs samples ratio of PGFs in GelMA was 2% w/v ( $\text{mg}/\mu\text{l}$ ). Comparison of stiffness, storage modulus ( $E'$ ) and loss modulus ( $E''$ ) between GelMA and GelMA-PGFs was carried out. The aspect ratio of the sample was kept consistent for all hydrogel tests to assure a similar loading mode. Uniaxial compression testing was conducted at room temperature using cyclic sinusoidal load mode to frequency oscillations, which varied from 0.05 to 20 Hz with 1 and 5 Hz intervals for GelMA and GelMA-PGFs. Samples were pre-loaded to 0.001 N force and dynamically tested at low deformation (0.1% strain) compression to ensure that the data collected was repeatable.

To determine the effect of photo-crosslinking time on Young's modulus of GelMA hydrogels ( $n = 3$ ), static compression mode was used to obtain stress/strain curves with ramp rate of 1 mm/min. Moduli were calculated from the slope of the linear region on the stress/strain curve using OriginPro 2019 of linear curve fitting.

## 2.8 | Crosslinking studies

The crosslinking time and effect of UV exposure on mechanical and biological performance of GelMA hydrogels was examined at 6 different time periods as 10, 20, 30, 60, 120, 300 s of UV exposure with the same conditions. XYZPrinting UV chamber (Model 3UD10, Taiwan, UV LED  $\lambda$  375–405 nm, 16 W) was used for photo-crosslinking. The assessment of mechanical properties was carried out with respect of Young's modulus via DMA, and cell metabolic activity and cell viability (Live/Dead assays) via alamarBlue assay and imaging on an inverted fluorescence microscope (Leica, DM IRB, UK), respectively. Methodological details for these tests were as described in previous related sections unless otherwise stated.

## 2.9 | Cell culture on PGFs laden GelMA hydrogels

GelMA hydrogel solution was prepared by dissolving freeze stored foams 10% (w/v) in PBS by magnetic stirring for 1 h at 35–40°C and then 0.1% (w/v) LAP was dissolved in the solution and stirred for a further  $\sim 15$  min. Afterwards, inside the laminar flow cabinet the hydrogel solution was sterilized via 0.22  $\mu\text{m}$  pore size syringe filtering by keeping the temperature slightly above 35°C. Harvested and quantified C6 glial cells were suspended GelMA hydrogel solution with a cell density of  $1 \times 10^5$  cells/ml to make a working stock solution of cell/hydrogel mixture. Sterilized 1 cm long, 5 mg mass of PGFs (PGFs – GelMA ratio kept at 2% w/v ( $\text{mg}/\mu\text{l}$ )), was placed into 48 well cell culture plates (Corning®, Labwares, UK) manual separation of fiber bundles was performed with the help of fine tipped tweezers and 250  $\mu\text{L}$  cell loaded hydrogel solution was casted around the PGFs and, and then all samples were crosslinked under UV light for 60 s and transferred into culture plates and cultured under 5%  $\text{CO}_2$  at 37°C. For comparison, the same number of cells were seeded on PGFs and placed into 1.5% agarose coated well plates. For cell adhesion morphology, the cells were stained with F-actin in all the groups and GelMA hydrogel without PGFs as control group.

## 2.10 | Phalloidin/DAPI staining

The cells adhesion and spreading behaviors were assessed by fluorescence microscopy observation. After 7–14 day of culturing, cells were fixed in 3.7% paraformaldehyde solution, washed in phosphate buffer solution (PBS) and followed by cell permeabilization by using 0.5% Triton X-100 solution, and washed in PBS again. Cytoskeletal and nuclei staining was performed with phalloidin (Alexa Fluor® 488 Phalloidin, Sigma-Aldrich, UK) and DAPI (Sigma-Aldrich, UK), respectively. Samples were immersed in the phalloidin dye for 20 min then washed twice with PBS, followed by immersing for 10 min in DAPI (300 nM in PBS) solution. This staining process was performed in the absence of light to reduce evaporation and photo bleaching of dye. Finally, stained cell morphologies were obtained using an inverted fluorescence

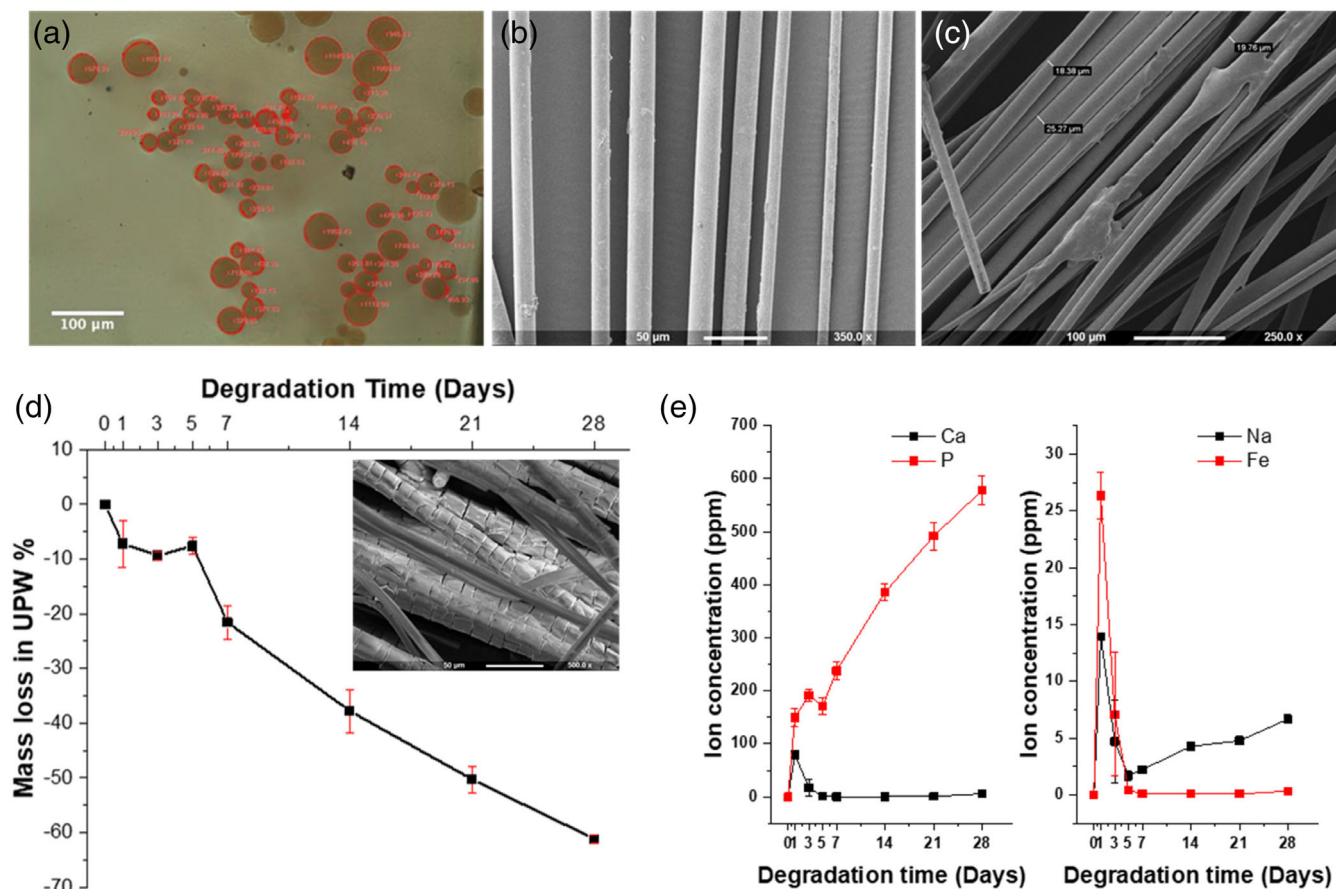


**FIGURE 1** Characterization of phosphate glass fibers (PGFs); (a) Diameter measurements of PGFs embedded in resin under optical microscope ( $n = 55$ ). (b–c) SEM images of PGFs for surface morphology assessment and diameter measurement. (d) Degradation profile of PGFs in term of mass change over time in UPW at  $37^{\circ}\text{C}$  ( $n = 3$ , for each time points). The inset SEM image of PGFs (after 14 days of immersion in DI) exhibits cracks occurring on the surface of PGFs. (e) The ions ( $\text{Ca}^{+2}$ ,  $\text{Na}^{+1}$ ,  $\text{P}^{+5}$ , and  $\text{Fe}^{+3}$ ) release profile in concentrations of Ca, P (left) Na, Fe (right) in ppm, from PGFs in water over 28 days ( $n = 3$ , for each time point)

microscope (Leica, DM IRB, UK). Further, all images were processed using ImageJ software.

## 2.11 | Statistical analysis

The data were analysed using one-way and two-way analysis of variance (ANOVA), with post hoc tests of Tukey's and Bonferroni's on OriginPro 2021. The  $p$  values were taken as an indicator of significant difference as follows for Figure 4(a)  $^*(p < 0.05)$  and  $^{**}(p < 0.01)$  and for Figure S2  $^*(p < 0.01)$ ,  $^{**}(p < 0.001)$ ,  $^{***}(p < 0.0001)$ .

## 3 | RESULTS

### 3.1 | Phosphate glass fibers (PGFs)

The average phosphate glass fiber diameters of  $20.17 \pm 7.19 \mu\text{m}$  were obtained using melt spinning at pulling speeds of 800 rpm (Figure 1(a)). The SEM image of PGFs showed an aligned microfibrus and smooth

surface morphology with average diameter of  $19.45 \pm 1.24 \mu\text{m}$  (Figure 1(b,c)), which is similar to the optical microscopy measurements. To produce PGFs diameter of  $20.17 \mu\text{m}$ , the rotation speed of drum was optimized as previously described by Ahmed et al.<sup>34</sup> The produced fibers average diameters were within the optimal range for neural cell attachment and spreading as the diameter of neural cell bodies are  $5\text{--}20 \mu\text{m}$ ,  $5\text{--}50 \mu\text{m}$  and up to  $50 \mu\text{m}$  for PC12 cells,<sup>35</sup> DRG neuronal cells, and glial cells,<sup>36,37</sup> respectively.

### 3.2 | Mass loss and ion release

The PGFs were further characterized for *in vitro* degradation by mean of mass loss and ion release test. The mass loss of the PGFs during the degradation test were monitored up to 28 days (Figure 1(d)). The degradation results showed a linear mass loss for an initial 2 weeks (up to 14 days,  $\sim 40\%$  mass loss) and the next two weeks showed slower degradation (14 days to 28 days,  $\sim 20\%$  mass loss), and a total of  $60\%$  mass loss at 28 days was observed. Moreover, the degradation of the PGFs also affects the fibers surface and cracks and breaks

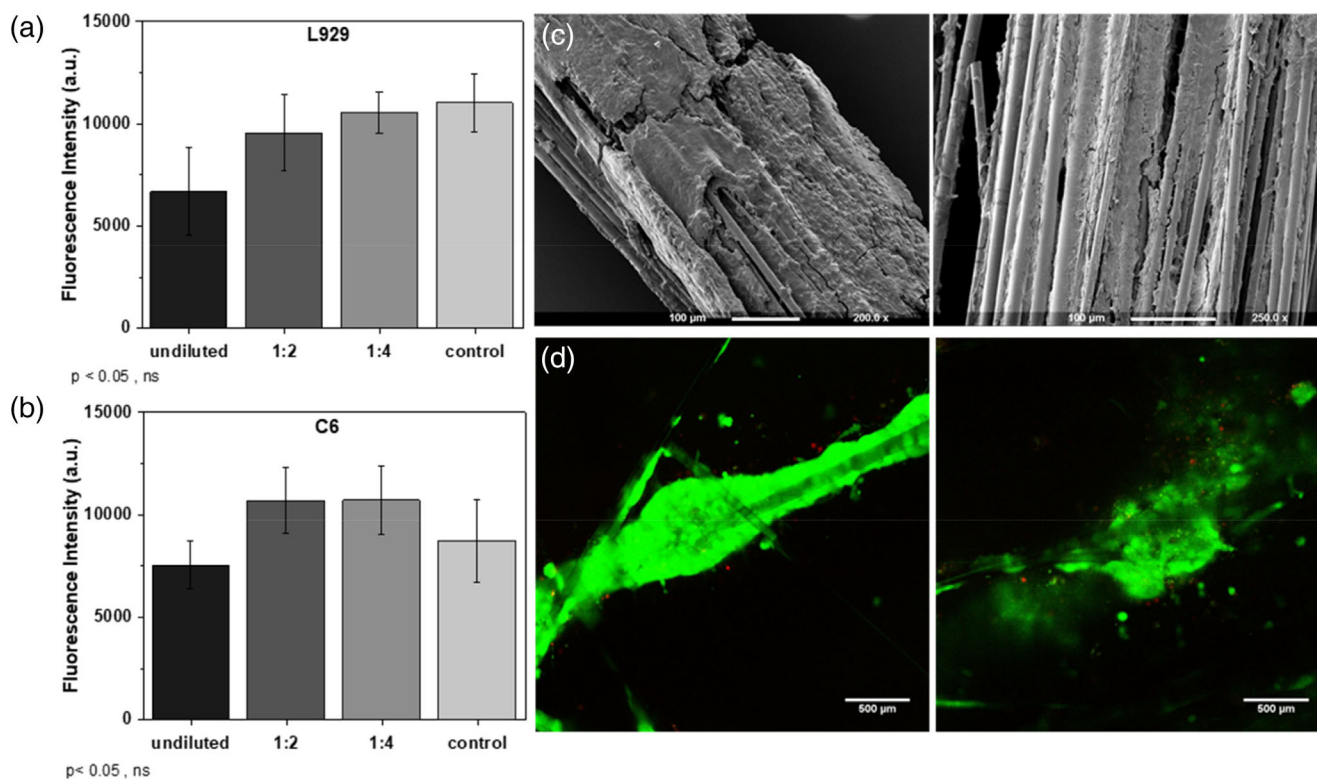


**FIGURE 2** Cytotoxicity, cell metabolic activity, adhesion, and viability assessments of PGFs; (a) Metabolic activity of L929 cells cultured on PGFs extraction for 24 h ( $n = 3$ ). (b) Metabolic activity of C6 cells cultured on PGFs extraction for 24 h ( $n = 3$ ). (c) SEM images of C6 cells attachment on PGFs surfaces after 14 days culture. (d) Cell viability by Live/Dead assay at 7 days of C6 cell culture on PGFs surface (scale bars 500 μm)

of fibers were observed by SEM (inset) surface analyses of five days immersed samples (Figure 1(d)). The initial fast (linear) degradation of PGFs mainly occurs due to water soluble ions via erosion/diffusion mechanism.

Along with the mass loss of PGFs in distilled water, the ion release from the PGFs were measured using ICP-OES. The ICP-OES data show that Ca, P, Na, and Fe ions are released from the PGFs ( $50\text{P}_2\text{O}_5 - 40\text{CaO} - 5\text{Na}_2\text{O}, 5\text{Fe}_2\text{O}_3$ ) (Figure 1(e)). The release profile of  $\text{Ca}^{+2}$ ,  $\text{P}^{+5}$ ,  $\text{Na}^{+1}$ , and  $\text{Fe}^{+3}$  ions are rapid for initial 3 days and showed  $\sim 80$ ,  $\sim 180$ ,  $\sim 12$ , and  $\sim 27$  ppm at 3 days, respectively. The release of Ca, Na, and Fe ions levelled off after 3 days, while P ion release rate was rather rapid and maintained linear profile between 5 and 28 days and the  $\text{P}^{5+}$  ion release during this period reached  $415 \pm 27$  ppm. The rapid initial release of ions from the PGFs was from the high presence of Ca (40 mol% CaO), and P (50 mol%  $\text{P}_2\text{O}_5$ ) contents and low presence of Na (5 mol%  $\text{Na}_2\text{O}$ ) and Fe (5 mol%  $\text{Fe}_2\text{O}_3$ ). The resultant calcium, phosphate, sodium, and iron ions at 28 days are  $\sim 100$ , 600, 35, and 42 ppm, respectively. The ion release results confirmed the initial fast degradation (mass loss) of the PGFs and mostly involved the Ca and P ions. Moreover, the degradation profile of PGFs can be easily altered by modification of the chemical composition via addition of oxides such as titanium dioxide ( $\text{TiO}_2$ ) into the glass structure to significantly slow the degradation rate.<sup>24</sup>

### 3.3 | *In vitro* cytotoxicity and biocompatibility of PGFs

The cytotoxicity of PGFs was evaluated by an extraction method according to ISO10993-5 standard. The undiluted extract from PGFs showed  $86 \pm 5.2\%$  viability compared to control (tissue culture plate; TCP) of culture media on L929 model fibroblast cell line. With the 1:2 and 1:4 diluted extracts cells showed significantly improved metabolic activity, but this was not statistically significant between groups (Figure 2(a)). The same was seen with the C6 cells which showed  $92 \pm 5.2\%$  viability with non-diluted extract exposure, diluted concentrations revealed positive effect on this cell line compare to control (Figure 2(b)). According to this method of cytotoxicity evaluation, cell viabilities greater than 70% have been determined as non-cytotoxic.<sup>32</sup> Thus, *in vitro* cell cytotoxicity results showed that the PGFs with undiluted, 1:2, and 1:4 diluted extract do not have a cytotoxic effect on L929 and C6 cells. The PGFs with C6 cell showed cell attachment on the PGFs surfaces at 24 h and cell morphology was observed by SEM (Figure 2(c)). The cell adhesion morphology showed complete coverage of glass fibers surface after 7 days of culture. Further, the viability of C6 cells was assessed up to 7 days of culture without any supplementary scaffolds or compound on to PGFs, and the viability of the cells was good in general and confocal images of the PGFs surfaces showed they were covered with cells (Figure 2(d)). Overall, *in*

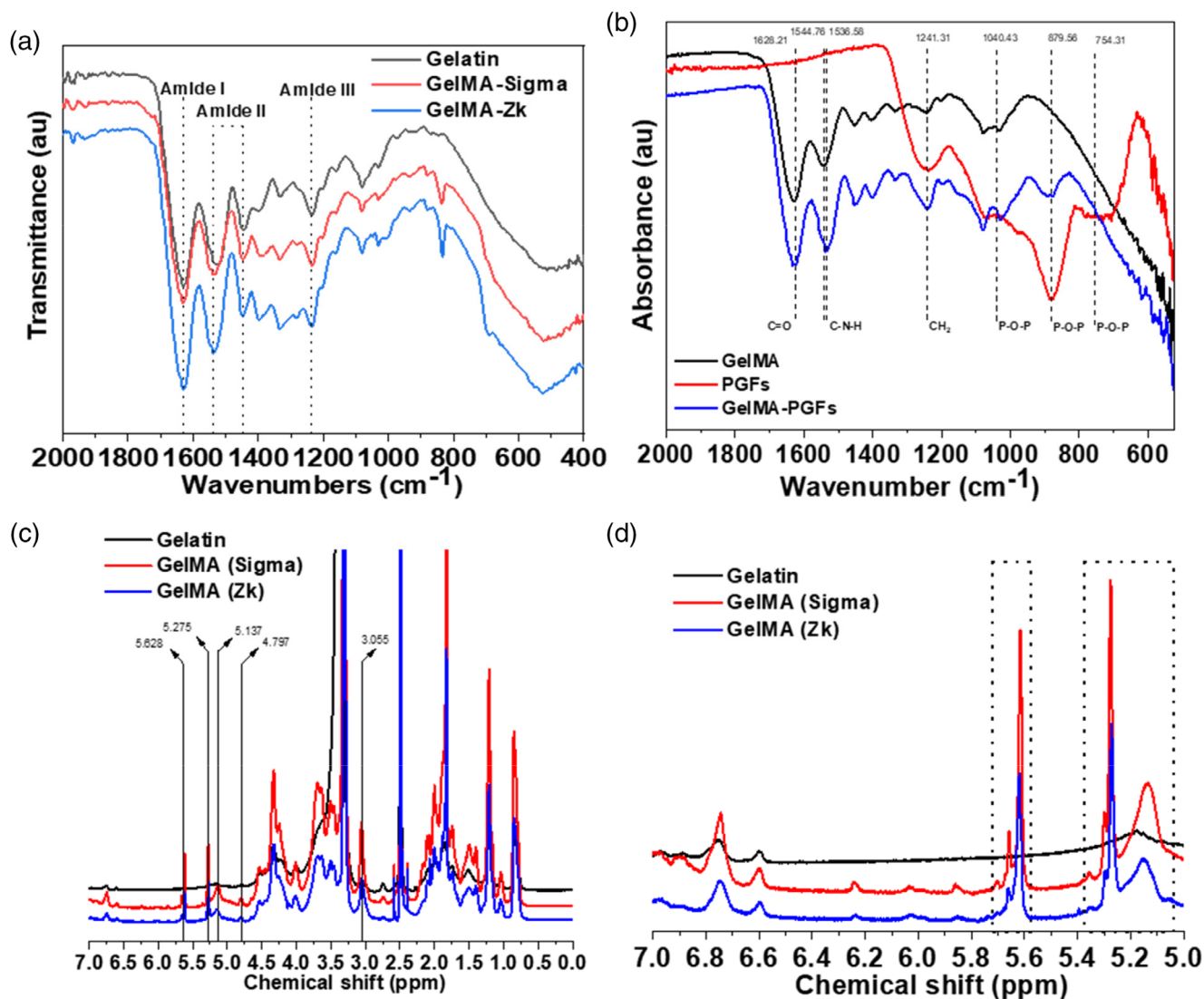


**FIGURE 3** Chemical characterizations of gelatin, GelMA and PGFs; FTIR and  $^1\text{H-NMR}$  characterizations (a) FTIR spectra of gelatin, GelMA (Sigma), and GelMA, (b) FTIR spectra of formulated GelMA, PGFs and GelMA-PGFs, (c) Medium range  $^1\text{H-NMR}$  spectra, and (d) short range  $^1\text{H-NMR}$  spectra. Vinyl groups of the MA were observed at the peaks at 5.275 and 5.628 ppm

*in vitro* cytotoxicity and biocompatibility results of PGFs with L929 and C6 cells confirmed that the fabricated PGFs are nontoxic and favourable for cell attachment and metabolic activity. Moreover, as in this case PGFs were not coated and surrounded by any gels or polymer but fibers stayed bundled as shown in the SEM and confocal images and it can be speculated that PGFs may allow the cells to deposit ECM and this may be of interest for fibers physical assembly via cellular modulation.

### 3.4 | GelMA characterization

GelMA was synthesized by modification of gelatin using MA to create polymers with the methacrylate substitution. ATR-FTIR spectrum of GelMA (Figure 3(a)) exhibits a strong peak for the primary amide (amide I) related C=O stretching groups appears at  $1650\text{ cm}^{-1}$  and

changes at the peak vibrations at  $1650\text{--}1670\text{ cm}^{-1}$  interval corresponds to C=C, C=O bonds that presents in the backbone of GelMA polymer the interaction between gelatin and methacrylate anhydride.<sup>38</sup> Shifts and changes determined in peaks of GelMA compared to gelatin indicate that gelatin has been successfully modified to GelMA and this has also been proved by comparing commercial GelMA product referred as GelMA-Sigma on Figure 3(a). Moreover on Figure 3(b), it has been shown that PGFs incorporation into GelMA has not interfered with amide bonds of GelMA while phosphate groups' stretches, (O - P - O), coming from PGFs can be seen at  $1000.43$ ,  $879.56$ , and  $754.31\text{ cm}^{-1}$ .<sup>39</sup>

$^1\text{H-NMR}$  spectra were used to quantify the amounts of methacrylate and methacrylamide groups in GelMA. The  $^1\text{H-NMR}$  spectra of gelatin, in house synthesized GelMA referred as (GelMA-Zk), and commercial GelMA referred as (GelMA-Sigma) were analyzed (Figure 3(b),(c)) and compare to gelatin spectra, GelMA-Zk, and

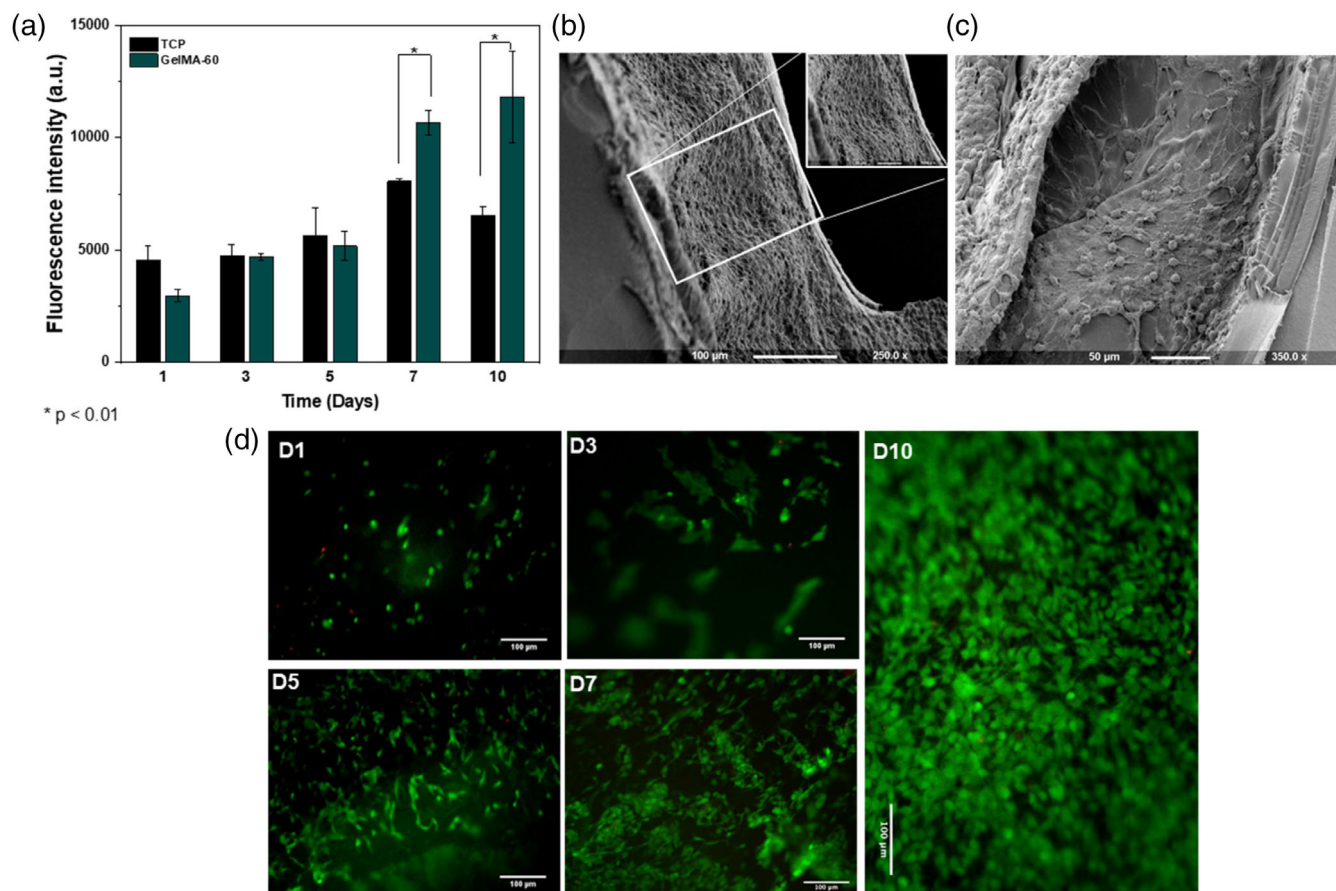


**FIGURE 4** 3D cell culture with GelMA hydrogel; (a) Metabolic activity of C6 cells cultured in GelMA-60 hydrogel at 1, 3, 5, 7, and 10 days by Alamar Blue assay (control is TCP) ( $n = 3$ ) (b–c) SEM image of cross-sectional area of cell laden GelMA-60 hydrogels at day 7 (D7). (d) Live&Dead fluorescence images of C6 cells into GelMA-60 hydrogels at D1,3,5,7–10 (Scale bars are 100 µm)

GelMA-Sigma exhibited three new proton peaks belonging to methacryloyl groups of GelMA between 6.2 and 5.2 ppm and at 1.9 ppm. Moreover, two major and highly intense new peaks were observed in GelMA-Zk and GelMA-Sigma in the range 5.71–5.57 ppm and 5.32–5.21 ppm (Figure 3(c)). Apparently the free lysine residues coming from unmodified gelatin seen at 3.0 ppm substantially decreased.<sup>20</sup> The synthesized GelMA was in close agreement to commercial GelMA (Sigma) which has 80% methacrylation degree. GelMA, with 86%, has demonstrated higher degree of substitution compared commercial GelMA (Figure 3(b),(c)).

### 3.5 | Mechanical and biological effects of crosslinking time

As a semi-synthetic material, it has been known that physiochemical properties of GelMA can be easily tailored by altering the degree of methacrylation and photo-crosslinking conditions.<sup>40</sup> In this study, a series of experiments were carried out to evaluate effects of UV exposure time for photo-crosslinking on mechanical properties and biological performance of GelMA hydrogels. The UV exposure time were selected from 10 to 300 s (10, 20, 30, 60, 120, and 300 s) of 6 different time points for the evaluation of mechanical properties in

terms of Young's, storage, and loss modulus, and biological performance in term of cells viability in the hydrogels (Figure 5(a), Figure S2). The biological performance of the GelMA hydrogel produced from different UV exposure times were carried out in 3D cell culture conditions and metabolic activity and live/dead assay up to 10 days to evaluate the long-term effects of UV were carried out (Figure S2(a),(b)).

The effects of UV exposure time on Young's modulus of GelMA hydrogel showed a gradual increase from  $\sim 375$  to  $1000 \text{ N/m}^2$  for 10 to 300 s, respectively (Figure 5(a)). With increased UV exposure time, a small increasing trend was also observed in the elasticity of GelMA hydrogels. The Young's modulus value for GelMA-10, GelMA-20, GelMA-30, GelMA-60, GelMA-120, and GelMA-300 were  $384 \pm 19$ ,  $403 \pm 66$ ,  $431 \pm 27$ ,  $526 \pm 50$ ,  $559 \pm 35$ , and  $1029 \pm 185 \text{ N/m}^2$ , respectively. The change in Young's modulus of 300 s UV exposed hydrogel termed as "GelMA-300" was significantly higher compared to all other time points. While the rest (GelMA-10, GelMA-20, GelMA-30, GelMA-60, and GelMA-120) did not show a statistically significant increase. The change in Young's modulus of GelMA hydrogel mainly depends on the parameters such as GelMA and PI concentrations, degree of methacrylation, and UV-exposure time and can be used to tailor the mechanical properties of the GelMA hydrogels.<sup>19-40</sup> The PI concentration is also crucial to optimize cell viability following

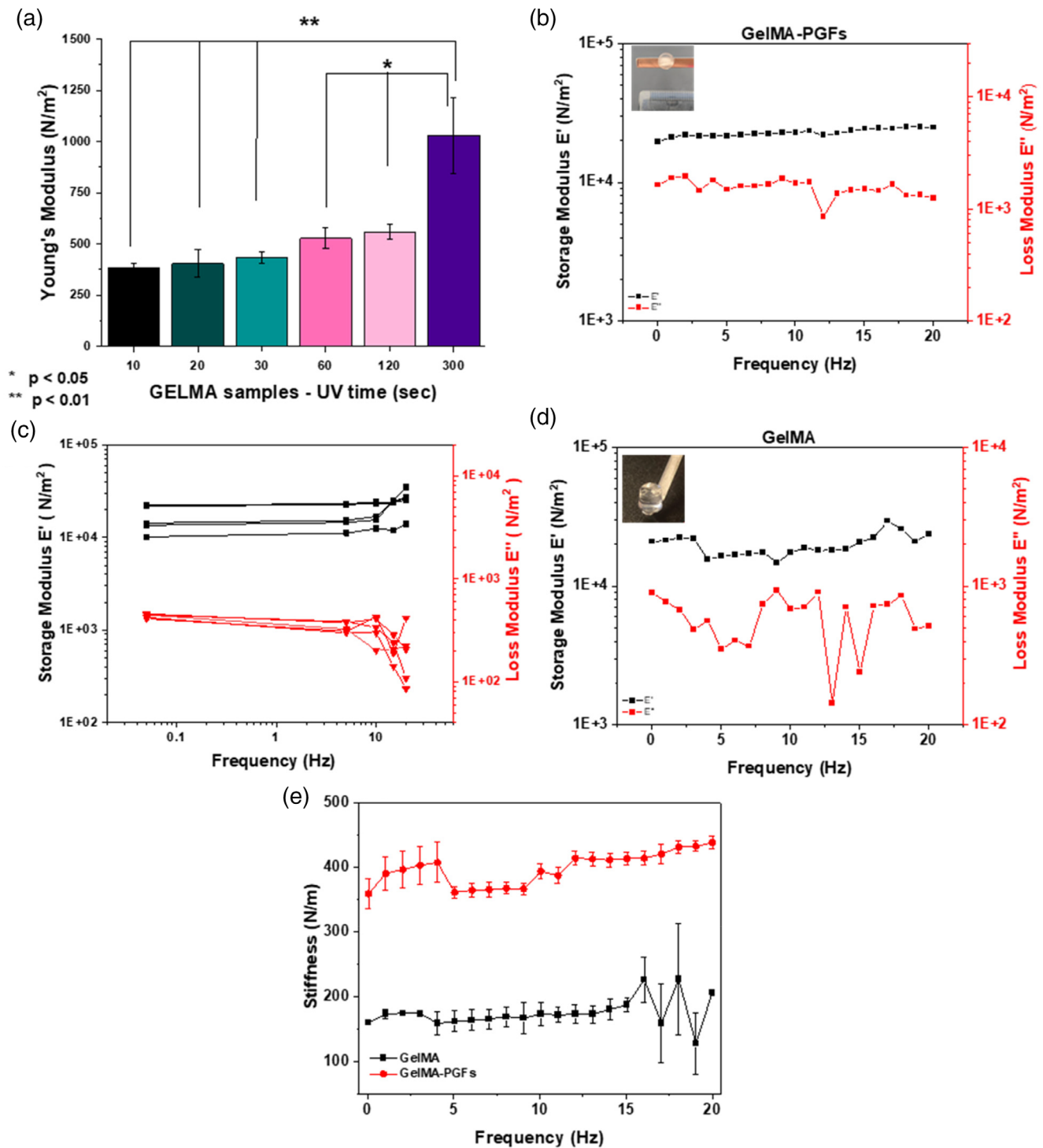


**FIGURE 5** Mechanical properties of GelMA, GelMA-PGFs; (a) Young's modulus of GelMA cured with different UV times DMA via static compression and calculated from the slope of linear region of stress/strain curve using OriginPro2019,  $n = 3$ ,  $p < 0.05$ ,  $**p < 0.01$  for significance, (b) Storage and Loss modulus of GelMA (60) five sweeps of frequency oscillations (c-d) Storage and Loss modulus measured of GelMA and GelMA-PGFs. with representative optical image of GelMA and GelMA-PGFs hydrogels crosslinked for 60 s UV (e) Stiffness of GelMA and GelMA-PGFs ( $n = 3$ )

crosslinking together with the consideration that lower levels of PI may require longer UV time to set hydrogel, so this balance needs to be optimized for the application. The key parameter is UV light flux which is a function depending on both PI concentration and UV-light intensity.<sup>40</sup> In this study, we have preferred to keep our PI

concentration at lower concentration (0.1% w/v) which showed high cell viability in 3D culture as well as showing easier and more homogeneous solubility in the hydrogel solution.

On the basis of viscoelastic properties and stiffness of GelMA and GelMA-PGFs hydrogels, we further chosen 60 s of UV

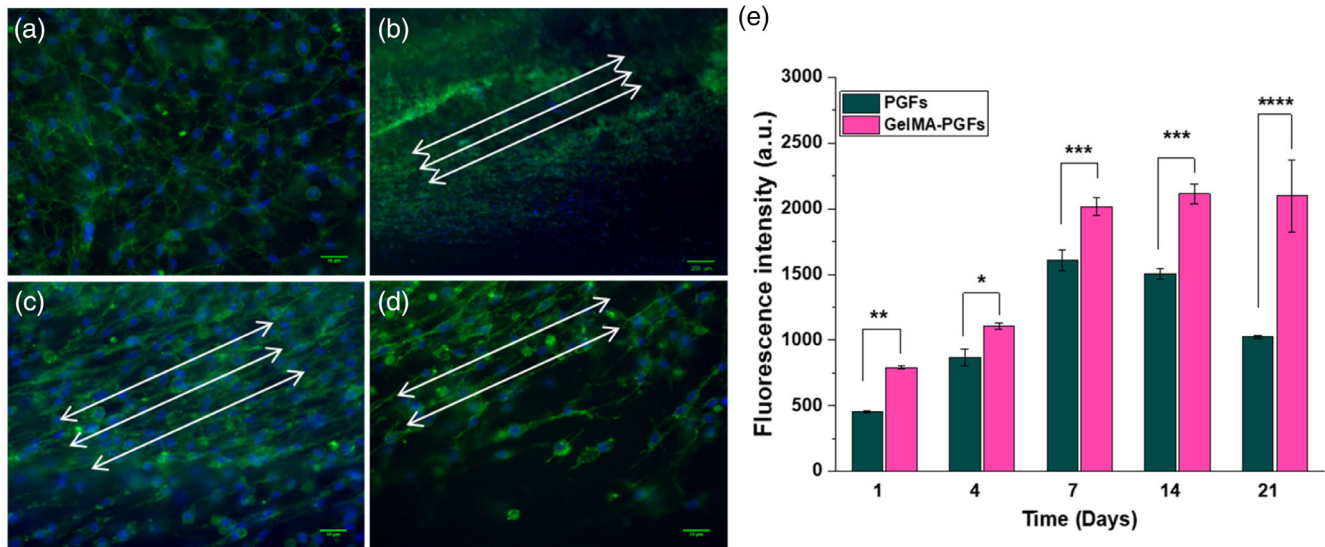


**FIGURE 6** Guided spreading and growth of C6 glial cells in PGFs laden GelMA-60 hydrogel and metabolic activity; (a) Phalloidin/DAPI staining of C6 cells into GelMA-60 hydrogel, (b–d) Phalloidin/DAPI staining of C6 cells into PGFs laden GelMA-60 hydrogel samples at day 14. Scale bars 50  $\mu\text{m}$  for a, c, d, for b 200  $\mu\text{m}$ . (e) Metabolic activity of C6 cells up to 21 days ( $n = 3$ ) \*  $p < 0.01$ , \*\*  $p < 0.001$ , and \*\*\*  $p < 0.0001$

exposure time. To evaluate storage modulus ( $E'$ ) and loss modulus ( $E''$ ) via DMA-uniaxial compression at a range of frequencies between 0.05 and 20 Hz at 1 and 5 Hz intervals, as over 10 Hz frequency due to possible microcracks in the hydrogel structure, and consequently, fluctuations in modulus values. The measurement of  $E'$  and  $E''$  were obtained which suggests that the elastic component measuring the stored energy and the viscous portion from the energy lost in the form of heat,<sup>41</sup> respectively. The  $E'$  and  $E''$  values for GelMA-60 hydrogel were recorded as function of frequency (Figure 5(a)). The  $E'$  and  $E''$  values were stable and constant between 0.05 to 10 Hz. The values of  $E'$  and  $E''$  for GelMA-60 hydrogel was  $24.73 \pm 2.52 \text{ kN/m}^2$  and  $1.08 \pm 0.23 \text{ kN/m}^2$ , respectively, which was considered suitable for application with soft and mild-soft tissues such as nerve and muscle.<sup>42,43</sup> As noticed, for all frequency values, the value of  $E'$  was higher than the  $E''$ , which indicates a predominantly elastic behavior rather than viscous behavior in the hydrogel structure.<sup>40</sup> The representative images of GelMA and GelMA-PGFs hydrogels are shown in the related graphs of Figure 5 (c),(d). As it can be seen on Figure 5(c),(d), PGFs incorporated GelMA has not shown a significant difference in viscoelastic behaviors however the fluctuation between frequency changes have clearly reduced due to a more stabilized and stiffer structure of the GelMA-PGFs (Figure 5(e)). PGFs incorporation into the GelMA has increased the stiffness of GelMA from  $174.37 \pm 14.1$  to  $396.99 \pm 6.33 \text{ N/m}$  as expected.

The biological behavior of the GelMA-60 hydrogel was evaluated by metabolic activity and cell viability. The metabolic activity of C6 cells in GelMA-60 hydrogel for initial timepoints showed no significant changes (Figure 4(a)). However, from D7 to D10 there was a decrease in metabolic activity control (TCP), which could be caused by the high confluency on TCP surface while it does not apply in 3D culture in GelMA. The high confluency leads to cell death and eventually reduces

the metabolic activity. However, the cells in the GelMA-PGFs have more room for proliferation and exhibit higher metabolic activity. The GelMA-60 hydrogel samples showed significantly better metabolic activity in the long term compared to control cells which were cultured on tissue culture plastic. The live & dead assay has showed qualitatively higher dead cell in day 1 for high UV exposure times like 60, 120, 300 s (Figure S2). Nonetheless, over time there was no major cell death and live cells increased in number (Figure 4(d)). The glial cells show radial growth in the GelMA-60 hydrogel sample at day 3 (D3) relatively quicker than other groups (Figure S2). Therefore, based on mechanical and biological performance of the GelMA-60 hydrogel sample have been chosen for the rest of the 3D cell culture studies with glial cells. In the long term, crosslinking conditions may have affected cell behavior in the hydrogels concerning changed mechanical characteristics of gels allied to alteration in degradation rate in parallel with the amount of photo-crosslinked methacrylate groups.

### 3.6 | Aligned growth of cells into PGFs laden GelMA-60

To investigate cellular cytoskeleton orientation and morphology of C6 cells in 3D cell culture of PGFs laden GelMA-60, phalloidin/DAPI histochemical staining was carried out after 14 days (D14) of cell culture (Figure 6). Radial glial morphology of the C6 cells can be seen in the images (Figure 6(a)–(d)). While cells in GelMA-60 hydrogel (no PGFs) have grown randomly into the hydrogel and exhibited no directional orientation, cells in the PGFs laden GelMA-60 hydrogels samples exhibited directional spreading and growth in the parallel direction of PGFs bundle at day 14 (D14) (Figure 6(b)–(d)). The direction of PGFs bundle in the GelMA-60 hydrogel have been indicated with white arrows on the images.

Long-term (up to 21 days) cell culture experiments were carried out with C6 cells on PGFs and into (3D) PGFs laden GelMA-60 hydrogels. The metabolic activity assessed by alamarBlue assay showed a gradual increase at all-time points in PGFs laden GelMA-60 hydrogel exhibited significantly higher rate compared to cell growth on PGFs surface (Figure 6(e)). As a hydrogel, GelMA has proved itself to be an attractive material that possesses excellent biological properties to support cell viability, proliferation, spreading and supporting cell-cell interactions and cell viability in usage of tissue engineering as scaffolds and/or cell carrier systems.<sup>49,50</sup>

## 4 | DISCUSSION

Viscoelasticity is an intrinsic property of a natural tissue and defines its unique mechanical niche. Thus, when developing new biomaterials for tissue engineering applications, mimicking the mechanical features of the target tissue should be considered.<sup>44</sup> Thanks to its tailorable mechanical properties photo crosslinked GelMA hydrogel which has great potential to be utilized for patient and injury specific tissue constructs for translational studies. Following spinal cord injury, glial scar formation creates a considerably stiffer surrounding site which this also can act as a mechanical barrier to neuronal regeneration<sup>45</sup> so by considering all environmental changes, and providing appropriate mechanical signal with permissive properties are crucial to design neural implants for enhanced functional recovery.<sup>46</sup> Regarding this with the presented DMA data, GelMA-PGFs has shown the potential to provide higher stiffness which can be tailored further with different ratios of PGFs in GelMA. Moreover, knowing that casting GelMA around PGFs may cause microenvironmental changes for cells around PGFs this has not affected the crosslinking of GelMA as shown on FTIR spectra in Figure 3(b).

In the light of inadequacies of two-dimensional (2D) cell culture systems for allowing mechanical cues to the cells in 3D cell culture with hydrogels have been used in tissue engineering for decades, therefore we have optimized our GelMA hydrogel system for 3D culturing of C6 cells (Figure 4). The SEM image of cell loaded GelMA-60 hydrogel samples cross-sectional area showed it was fully covered with grown cells at day 7 (D7) (Figure 4(b),(c)).

Thanks to their superior swelling properties and biocompatibility hydrogels provides a good permissive environment to cells for nutrient and gas exchange for long term cell culture studies.<sup>16,47,48</sup> Hence performing 3D experiments with hydrogels are good steps before planning *in vivo* experiments.

East et al. have studied on 3D collagen model system to provide astrocyte alignment for neural recoveries followed by SCI, they have reported that providing aligned astrocyte growth enhanced neurite outgrowths.<sup>51</sup> Joo et al. have worked with similar approaches for PGFs-collagen scaffolds for SCI recoveries and showed for the first time the efficiency of PGFs in nerve regeneration following SCI. Their results showed that the presence of glass fibers in the scaffold improved the recovery of locomotor functions compared to collagen only scaffolds after eight weeks of implantation.<sup>30</sup> Despite its excellent biological performance collagen as a biomaterial has mechanically

poor properties to handle and work with. However, GelMA can be a good alternative to collagen in terms of it being easy to modify the structure and relatively superior mechanical properties. In addition, in the present study, the perspective of directionality for neural tissue has been projected with glial cells rather than neurons as commonly evaluated. As such this may offer a promising model system in terms of understanding supportive roles of astrocytes and glia in the site and their importance of alignment for axonal regeneration.

Recent studies been reviewing that although approaches like cell therapies including stem cells or neural progenitor cell transplantation targeting CNS recoveries are promising, extra physical support also needs to be provided using biomaterial scaffolds for connectivity and supporting cytoarchitecture.<sup>15,52,53</sup> Therefore, there is still a need to construct the optimal biomaterial systems to address physical and mechanical needs for CNS regeneration, specifically for acute and chronic SCI. For ultimate applications of the scaffold to bridge gaps in SCIs specific constructs may be needed, thus it can be advantageous to use a base biomaterial like GelMA hydrogel, its properties can be easily tailored, including bio-printability. Joung et al. have studied 3D printed stem-cell derived scaffolds for SCI by using mixed bioink of Matrigel/Gelatine/Fibrin and GelMA and reported that their printing platform could generate biomimetic scaffolds for complex CNS tissue models *in vitro*.<sup>9</sup> Koffler et al. have emphasized that numerous bio-engineered scaffolds targeting SCI unmet to address host inflammatory responses and their presented biomimetic 3D printed PEGDA-GelMA scaffold that can regulate astrocyte response in the injured site by aligning host astrocytes.<sup>54</sup> The alignment of cells in the injury site when supported with mitigated environmental changes can be associated with functional neural recovery.<sup>51-55</sup>

In this study, the results have shown that PGFs degrades by ~60 wt% in 28 days in aqueous environment though it maintained directionality (Figure 1(d)), Vitale-Brovarene et al.<sup>56</sup> indicated in their work as well, the degradation profile of PGFs in aqueous environment is advantageous since glass fibers maintain their structural integrity. This would provide an important aspect for biomedical applications and particularly in this study maintaining biophysical cue for aligned growth of cells. Structural integrity can be the major limitation of GelMA-PGFs system from both materials' sides that can be investigated further in terms of changing composition, size, and concentration of PGFs and degree of substitution of GelMA. In addition, instead of iron as used in this work, it is possible to incorporate other specific ions showing antibacterial and antioxidant properties to the glass composition such as silver, zinc, copper, titanium that can be useful to occurring processes and pathophysiology of injury.

Apart from providing directionality, the presence of PGFs could be beneficial for better tailoring of mechanical properties as well as degradation kinetics of the constructs as such additions of PGFs to GelMA structure with the amount of 2 mg per 100  $\mu$ l gel, has increased the stiffness of scaffold more than twice as much (Figure 5(e)).

In the presented *in vitro* works although the images were taken on day 14 to show the clear alignment of C6 cells, the stimulation of guidance with PGFs was seen from the beginning of culture. Further quantitative measures need to be applied to determine whether alignment of cells starts early in the culture.

## 5 | CONCLUSIONS

This study showed the development and characterization of GelMA and PGFs for neural tissue engineering applications. PGFs structured GelMA hydrogels have shown potential to promote directional growth of glial cells that can be advantageous to encourage nerve repair in SCIs.

In conclusion, the results from this study offer a promising system combining the benefits of a hydrogel system constructed with GelMA and PGFs which are known to direct and drive neural cell axial growth, making them highly beneficial for SCI. In this sense our system is particularly promising as it provides directionality with glial cells and tuneable mechanical and biological properties via the materials. Further simple casting models have been developed to move to translational studies (Figure S1). Moreover, a combination of PGFs systems with hydrogels will provide easy usage of fibers for transplantation applications as well as their promising biological properties.

Our future studies will, therefore, explore changing composition and/or diameter of the PGFs and the hydrogels by addressing SCI induced environmental changes for potential translational works.

### ACKNOWLEDGMENTS

Funding for the PhD studies of first author Zaliye Keskin-Erdogan have been providing by Turkish Ministry of National Education with the awarded scholarship of Selection & Placement of Students to be sent abroad for post graduate studies (YLSY). The authors would also like to acknowledge the funding of National Research Foundation of Korea (Program for UCL Eastman-Korea Dental Medicine Innovation Centre; 2018K1A4A3A0106425) and (NRF; 2018R1D1A1B07048020). Furthermore, we would like to thank Dr Nicola Mordan, Dr George Georgeou, Dr Graham Palmer for their technical support with SEM, DMA and ICP-OES, respectively.

### CONFLICTS OF INTEREST

The authors have no competing financial interests on this study.

### DATA AVAILABILITY STATEMENT

The data that support the findings of this study are available from the corresponding author, [JCK], upon reasonable request

### ORCID

Zaliye Keskin-Erdogan  <https://orcid.org/0000-0001-6789-6954>

David Y.S. Chau  <https://orcid.org/0000-0001-9200-6749>

### REFERENCES

- Bradbury EJ, Burnside ER. Moving beyond the glial scar for spinal cord repair. *Nat Commun*. 2019;10:3879. <https://doi.org/10.1038/s41467-019-11707-7>.
- Ghorbani F, Zamanian A. Oriented microstructure in neural tissue engineering: a review. *J Tissue Sci Eng*. 2016;07(03):1000182. <https://doi.org/10.4172/2157-7552.1000182>.
- Huang Y-C, Huang Y-Y. Tissue engineering for nerve repair. *Biomed Eng Appl Basis Commun*. 2006;18(03):100-110. <https://doi.org/10.4015/S101623720600018X>.
- Grinsell D, Keating CP. Peripheral nerve reconstruction after injury: a review of clinical and experimental therapies. *Biomed Res Int*. 2014;2014:1-13. <https://doi.org/10.1155/2014/698256>.
- Mothe AJ, Tator CH. Review of transplantation of neural stem/progenitor cells for spinal cord injury. *Int J Dev Neurosci*. 2013;31(7):701-713. <https://doi.org/10.1016/j.ijdevneu.2013.07.004>.
- Reis KP, Sperling LE, Teixeira C, et al. VPA/PLGA microfibers produced by coaxial electrospinning for the treatment of central nervous system injury. *Braz J Med Biol Res*. 2020;53(4):e8993. <https://doi.org/10.1590/1414-431x20208993>.
- Niemczyk B, Sajkiewicz P, Kolbuk D. Injectable hydrogels as novel materials for central nervous system regeneration. *J Neural Eng*. 2018;15(5):051002. <https://doi.org/10.1088/1741-2552/aacbab>.
- Wei Z, Zhao J, Chen YM, Zhang P, Zhang Q. Self-healing polysaccharide-based hydrogels as injectable carriers for neural stem cells. *Sci Rep*. 2016;6:37841. <https://doi.org/10.1038/srep37841>.
- Joung D, Truong V, Neitzke CC, et al. 3D printed stem-cell derived neural progenitors generate spinal cord scaffolds. *Adv Funct Mater*. 2018;28(39):1-10. <https://doi.org/10.1002/adfm.201801850>.
- Dumont CM, Carlson MA, Munsell MK, et al. Aligned hydrogel tubes guide regeneration following spinal cord injury. *Acta Biomater*. 2019;86:312-322. <https://doi.org/10.1016/j.actbio.2018.12.052>.
- Wu Y, Xiang Y, Fang J, et al. A biocompatible hydrogel with improved stiffness and hydrophilicity for modular tissue engineering assembly. *Materials*. 2017;5(12):731-741. <https://doi.org/10.3390/jms18122675>.
- Meng F, Modo M, Badylak SF. Biologic scaffold for CNS repair. *Regen Med*. 2014;9(3):367-383. <https://doi.org/10.2217/rme.14.9>.
- Prager J, Adams CF, Delaney AM, et al. Stiffness-matched biomaterial implants for cell delivery: clinical, intraoperative ultrasound elastography provides a 'target' stiffness for hydrogel synthesis in spinal cord injury. *J Tissue Eng*. 2020;11:1-14. <https://doi.org/10.1177/2041731420934806>.
- Tam RY, Fuehrmann T, Mitrousis N, Shoichet MS. Regenerative therapies for central nervous system diseases: a biomaterials approach. *Neuropsychopharmacology*. 2014;39(1):169-188. <https://doi.org/10.1038/npp.2013.237>.
- Wang Y, Tan H, Hui X. Biomaterial scaffolds in regenerative therapy of the central nervous system. *BioMed Res Int*. 2018;2018:7848901. <https://doi.org/10.1155/2018/7848901>.
- Zhong Y, Bellamkonda RV. Biomaterials for the central nervous system. *J Royal Soc Interface*. 2008;5(26):957-975. <https://doi.org/10.1098/rsif.2008.0071>.
- Van Den Bulcke AI, Bogdanov B, De Rooze N, Schacht EH, Cornelissen M, Berghmans H. Structural and rheological properties of methacrylamide modified gelatin hydrogels. *Biomacromolecules*. 2000;1:31-38. <https://doi.org/10.1021/bm990017d>.
- Pepelanova I, Kruppa K, Scheper T, Lavrentieva A. Gelatin-Methacryloyl (GelMA) hydrogels with defined degree of functionalization as a versatile toolkit for 3D cell culture and extrusion bioprinting. *Bioengineering*. 2018;5(3):55. <https://doi.org/10.3390/bioengineering5030055>.
- Sun M, Sun X, Wang Z, Guo S, Yu G, Yang H. Synthesis and properties of gelatin methacryloyl (GelMA) hydrogels and their recent applications in load-bearing tissue. *Polymers*. 2018;10(11):1290. <https://doi.org/10.3390/POLYM10111290>.
- Zhu M, Wang Y, Ferracci G, Zheng J, Cho NJ, Lee BH. Gelatin methacryloyl and its hydrogels with an exceptional degree of controllability and batch-to-batch consistency. *Sci Rep*. 2019;9(1):1-13. <https://doi.org/10.1038/s41598-019-42186-x>.
- Diaz-Gomez L, Elizondo ME, Koons GL, et al. Fiber engraving for bioink bioprinting within 3D printed tissue engineering scaffolds. *Bio-printing*. 2020;18(2020):e00076. <https://doi.org/10.1016/j.bprint.2020.e00076>.
- Kim W, Kim G. 3D bioprinting of functional cell-laden bioinks and its application for cell-alignment and maturation. *Appl Mater Today*. 2020;19(2020):100588. <https://doi.org/10.1016/j.apmt.2020.100588>.
- Knowles JC. Phosphate based glasses for biomedical applications. *J Mater Chem*. 2003;13(10):2395-2401. <https://doi.org/10.1039/b307119g>.

24. Kiani A, Lakhkar NJ, Salih V, et al. Titanium-containing bioactive phosphate glasses. *Philos Trans A Math Phys Eng Sci.* 2012;370(1963):1352-1375. <https://doi.org/10.1098/rsta.2011.0276>.
25. Lakhkar NJ, Park JH, Mordan NJ, et al. Titanium phosphate glass microspheres for bone tissue engineering. *Acta Biomater.* 2012;8(11):4181-4190. <https://doi.org/10.1016/j.actbio.2012.07.023>.
26. Ahmed I, Abou Neel EA, Valappil SP, et al. The structure and properties of silver-doped phosphate-based glasses. *J Mater Sci.* 2007;42(23):9827-9835. <https://doi.org/10.1007/s10853-007-2008-9>.
27. Ahmed I, Collins CA, Lewis MP, Olsen I, Knowles JC. Processing, characterization and biocompatibility of iron-phosphate glass fibers for tissue engineering. *Biomaterials.* 2004;25(16):3223-3232. <https://doi.org/10.1016/j.biomaterials.2003.10.013>.
28. Kaur M. Optical and structural properties of cerium doped zinc phosphate glasses. *I-Manager's J Mater Sci.* 2018;5(4):30-36.
29. Foroutan F, McGuire J, Gupta P, et al. Antibacterial copper-doped calcium phosphate glasses for bone tissue regeneration. *ACS Biomater Sci Eng.* 2019;5(11):6054-6062. <https://doi.org/10.1021/acsbomaterials.9b01291>.
30. Joo NY, Knowles JC, Lee GS, et al. Effects of phosphate glass fiber-collagen scaffolds on functional recovery of completely transected rat spinal cords. *Acta Biomater.* 2012;8(5):1802-1812. <https://doi.org/10.1016/j.actbio.2012.01.026>.
31. Lin J, Jo SB, Kim TH, Kim HW, Chew SY. RNA interference in glial cells for nerve injury treatment. *J Tissue Eng.* 2020;11:2041731420939224. <https://doi.org/10.1177/2041731420939224>.
32. Biological Evaluation of Medical Devices, Biomedical Safety & Standards. 1996;26(7):54. <https://doi.org/10.1097/00149078-199604150-00011>.
33. Basara G, Yue X, Zorlutuna P. Dual crosslinked gelatin methacryloyl hydrogels for photolithography and 3D printing. *Gels.* 2019;5(3):34.
34. Ahmed, I., Lewis, M., Olsen, I., & Knowles, J. C. (2004). Phosphate glasses for tissue engineering: part 2. Processing and characterization of a ternary-based P2O5-CaO-Na 2O glass fibre system. *Biomaterials,* 25(3), 501-507. [https://doi.org/10.1016/S0142-9612\(03\)00547-7](https://doi.org/10.1016/S0142-9612(03)00547-7)
35. Fujita K, Lazarovici P, Guroff G. Regulation of the differentiation of PC12 pheochromocytoma cells. *Environ Health Perspect.* 1989;80:127-142. <https://doi.org/10.1289/ehp.8980127>.
36. Ahn HS, Hwang JY, Kim MS, et al. Carbon-nanotube-interfaced glass fiber scaffold for regeneration of transected sciatic nerve. *Acta Biomater.* 2015;13:324-334. <https://doi.org/10.1016/j.actbio.2014.11.026>.
37. Parent A, Carpenter MB. *Carpenter's human neuroanatomy.* 9th, Rose Tree Corporate Center, Building II 1400. Providence Rd. Suite 5025 Media, PA 19063-2043. Williams & Wilkins; 1996.
38. Rahali K, Ben Messaoud G, Kahn CJF, et al. Synthesis and characterization of nanofunctionalized gelatin methacrylate hydrogels. *Int J Mol Sci.* 2017;18(12):2675. <https://doi.org/10.3390/ijms18122675>.
39. Tan C, Rudd C, Parsons A, et al. Chitosan as a coupling agent for phosphate glass fibre/polycaprolactone composites. *Fibers.* 2018;6(4):97. <https://doi.org/10.3390/fib6040097>.
40. O Connell CD, Zhang B, Onofrillo C, et al. Tailoring the mechanical properties of gelatin methacryloyl hydrogels through manipulation of the photocrosslinking conditions. *Soft Matter.* 2018;14(11):2142-2151. <https://doi.org/10.1039/c7sm02187a>.
41. Buitrago JO, Patel KD, El-Fiqi A, et al. Silk fibroin/collagen protein hybrid cell-encapsulating hydrogels with tunable gelation and improved physical and biological properties. *Acta Biomater.* 2018;69:218-233. <https://doi.org/10.1016/j.actbio.2017.12.026>.
42. Koser DE, Moeendarbary E, Hanne J, Kuerten S, Franze K. CNS cell distribution and axon orientation determine local spinal cord mechanical properties. *Biophys J.* 2015;108(9):2137-2147. <https://doi.org/10.1016/j.bpj.2015.03.039>.
43. Karimi A, Shojaei A, Tehrani P. Mechanical properties of the human spinal cord under the compressive loading. *J Chem Neuroanat.* 2017;86:15-18. <https://doi.org/10.1016/j.jchemneu.2017.07.004>.
44. Huang D, Huang Y, Xiao Y, et al. Viscoelasticity in natural tissues and engineered scaffolds for tissue reconstruction. *Acta Biomater.* 2019;97:74-92. <https://doi.org/10.1016/j.actbio.2019.08.013>.
45. Moeendarbary E, Weber IP, Sheridan GK, et al. The soft mechanical signature of glial scars in the central nervous system. *Nat Commun.* 2017;8:1-11. <https://doi.org/10.1038/ncomms14787>.
46. Pampaloni F, Reynaud EG, Stelzel EHK. The third dimension bridges the gap between cell culture and live tissue. *Nat Rev Mol Cell Biol.* 2007;8(10):839-845. <https://doi.org/10.1038/nrm2236>.
47. Wei D, Xiao W, Sun J, et al. A biocompatible hydrogel with improved stiffness and hydrophilicity for modular tissue engineering assembly. *J Mater Chem B.* 2015;3(14):2753-2763. <https://doi.org/10.1039/c5tb00129c>.
48. Yahia L. History and applications of hydrogels. *J Biomed Sci.* 2017;04(02):1-23. <https://doi.org/10.4172/2254-609x.100013>.
49. Drury, J. L., & Mooney, D. J. (2003). Hydrogels for tissue engineering: scaffold design variables and applications. *Biomaterials,* 24(24), 4337-4351. [https://doi.org/10.1016/S0142-9612\(03\)00340-5](https://doi.org/10.1016/S0142-9612(03)00340-5)
50. Hunt JA, Chen R, Van Veen T, Bryan N. Hydrogels for tissue engineering and regenerative medicine. *J Mater Chem B.* 2014;2(33):5319-5338. <https://doi.org/10.1039/c4tb00775a>.
51. East E, De Oliveira DB, Golding JP, Phillips JB. Alignment of astrocytes increases neuronal growth in three-dimensional collagen gels and is maintained following plastic compression to form a spinal cord repair conduit. *Tissue EngPart A.* 2010;16(10):3173-3184. <https://doi.org/10.1089/ten.tea.2010.0017>.
52. Hong LTA, Kim YM, Park HH, et al. An injectable hydrogel enhances tissue repair after spinal cord injury by promoting extracellular matrix remodeling. *Nat Commun.* 2017;8(533). <https://doi.org/10.1038/s41467-017-00583-8>.
53. Gostynska N, Shankar Krishnakumar G, Campodoni E. Bioamine-crosslinked gellan gum hydrogel for neural tissue engineering related content 3D porous collagen scaffolds reinforced by glycation with ribose for tissue engineering application. *Biomed Mater.* 2017;12:025014. <https://doi.org/10.1088/1748-605X/aa62b0>.
54. Koffler J, Zhu W, Qu X, et al. Biomimetic 3D-printed scaffolds for spinal cord injury repair. *Nat Med.* 2019;25(2):263-269. <https://doi.org/10.1038/s41591-018-0296-z>.
55. Thompson R, Sakiyama-Elbert S. Using biomaterials to promote pro-regenerative glial phenotypes after nervous system injuries. *Biomed Mater (Bristol).* 2018;13(2):024104. <https://doi.org/10.1088/1748-605X/aa9e23>.
56. Vitale-Brovarene C, Novajra G, Lousteau J, Milanese D, Raimondo S, Fornaro M. Phosphate glass fibres and their role in neuronal polarization and axonal growth direction. *Acta Biomater.* 2012;8(3):1125-1136. <https://doi.org/10.1016/j.actbio.2011.11.018>.

## SUPPORTING INFORMATION

Additional supporting information may be found online in the Supporting Information section at the end of this article.

**How to cite this article:** Keskin-Erdogan Z, Patel KD, Chau DYS, Day RM, Kim H-W, Knowles JC. Utilization of GelMA with phosphate glass fibers for glial cell alignment. *J Biomed Mater Res.* 2021;1-13. <https://doi.org/10.1002/jbm.a.37206>